

## Are groundwater inputs into river-dominated areas important? The Chao Phraya River—Gulf of Thailand

H. Dulaiova<sup>1</sup> and W. C. Burnett

Department of Oceanography, Florida State University, Tallahassee, Florida 32306

G. Wattayakorn and P. Sojisuporn

Department of Marine Science, Faculty of Science, Chulalongkorn University, Bangkok 10330, Thailand

### Abstract

We used the natural geochemical tracers radon-222 and radium isotopes ( $^{223}\text{Ra}$ ,  $^{224}\text{Ra}$ ,  $^{226}\text{Ra}$ ,  $^{228}\text{Ra}$ ) to assess exchange rates between the Chao Phraya River and the Gulf of Thailand, and the magnitude of groundwater discharge in the estuary. We performed tracer surveys during two periods in 2004, in January (dry season, gauged river discharge  $47\text{ m}^3\text{ s}^{-1}$ ) and in July (wet season,  $430\text{ m}^3\text{ s}^{-1}$ ). The isotopic data suggested that there are at least three different sources of these tracers in the estuary: river water, seawater, and groundwater. We estimated the extent of each input via a mixing model using  $^{222}\text{Rn}$ ,  $^{223}\text{Ra}$ , and  $^{224}\text{Ra}$  activities and  $^{224}\text{Ra} : ^{223}\text{Ra}$  ratios. Our analysis showed that the largest groundwater outflow occurs near the mouth of the river. Our groundwater discharge estimates based on the mixing model are  $10$  and  $16\text{ m}^3\text{ s}^{-1}$  for January and July, respectively. An independent estimate of groundwater discharge in July using a mass balance of excess  $^{226}\text{Ra}$  together with our estimated water exchange rates based on  $^{224}\text{Ra} : ^{223}\text{Ra}$  ratios resulted in a range of  $14$ – $19\text{ m}^3\text{ s}^{-1}$ , depending upon the estimated amount of desorbable radium. Our estimated groundwater inputs therefore represent about 20% of the river flow during low flow in January and 4% during high flow conditions in July 2004. The unit shoreline flux ( $\sim 200\text{ m}^3\text{ m}^{-1}\text{ d}^{-1}$  in July) for the area around the river mouth is over one order of magnitude higher than two other areas of the Gulf of Thailand where groundwater fluxes have been evaluated.

Groundwater discharge is recognized as a significant, but poorly quantified, source of nutrients and dissolved species to coastal waters and estuaries. It may also be a pathway for land-derived contaminants of anthropogenic origin. One of the geographic areas where groundwater transport to the marine environment has been scarcely studied but could be particularly important is in Southeast Asia. The area has a wet climate and large regions are covered by limestone terrains that are particularly conducive to underground flow. An understanding of submarine groundwater discharge (SGD) is needed especially because many countries in the region are undergoing rapid agricultural and industrial development. Such activities may have a significant effect on surface and groundwater chemistry with potential influence on the water quality and ecology of the coastal zone.

<sup>1</sup>Current address: Woods Hole Oceanographic Institution, Woods Hole, Massachusetts 02543.

### Acknowledgments

We thank the crew of the R/V *Chula Vijai* for their helpful assistance during the river-estuary cruises. Supitcha Chanyotha and others from the Nuclear Technology Department, Engineering Faculty, Chulalongkorn University provided some of the well sampling and radon analyses. Peter Fuleky helped with the mixing model computation. We thank Billy Moore for his helpful comments on the mixing model. We thank the two anonymous reviewers for their fair and constructive comments. The investigators thank the Southeast Asia Regional Committee for System for Analysis, Research, and Training for the initial financial assistance that made this research possible. The authors from Florida State University acknowledge the support from the National Science Foundation (award OCE03-50514).

In recent years, progress has been made in the number of SGD investigations on different types of coastal zones. However, the importance of groundwater inputs in river-dominated margins is still an open question. Identification of SGD in a region with large riverine inputs is challenging since the geochemical signals may be similar. Moore (1997), Krest et al. (1999), and Moore and Krest (2004) have identified groundwater discharge in the Mississippi, Atchafalaya, and Ganges–Brahmaputra estuaries using radium isotopes.

The most widely used methods of assessment of SGD are direct measurement techniques (seepage meters), hydrological modeling, and the application of geochemical tracers (Burnett et al. 2001b; Taniguchi et al. 2002). Radon and radium isotopes are the most frequently used geochemical tracers.  $^{222}\text{Rn}$  is a naturally occurring radioactive element with a half-life of 3.8 d. It is a nonreactive noble gas and its only losses from the water column are due to its radioactive decay and evasion to the atmosphere. Because groundwater is in contact with radon-emanating aquifer material,  $^{222}\text{Rn}$  concentrations in groundwater are often about two to three orders of magnitude higher than most surface waters. This makes radon very useful in identifying areas of groundwater input into lakes, rivers, and the coastal ocean, and it can be used to estimate the dynamics and magnitude of groundwater discharge (Cable et al. 1996; Burnett et al. 2002; Burnett and Dulaiova 2003).

Naturally occurring radium isotopes are also used as tracers of SGD (Moore 1996; Charette et al. 2001; Kelly and Moran 2002) and are widely applied to study estuarine and coastal mixing rates. The distribution and flux of radium isotopes in estuaries have been investigated by

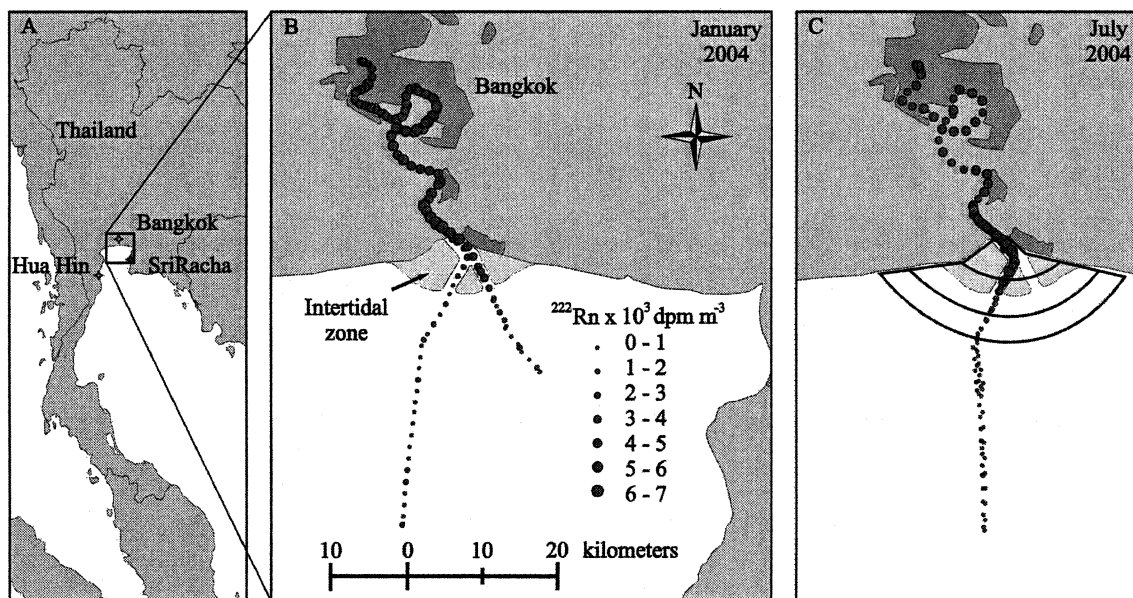


Fig. 1. (A) Map of Thailand depicting the upper Gulf of Thailand; (B) Chao Phraya River with the January 2004 radon data; (C) July 2004 trajectories. Radon ( $^{222}\text{Rn}$ ) activities measured in the near-surface waters are plotted on the transects where larger circles represent higher activities. Towns of Hua Hin and Sri Racha indicated in A were our two additional study sites. The semicircle patterns (C) are used for the  $^{226}\text{Ra}$  mass balance (see text).

many investigators, including Li et al. (1977), Krest et al. (1999), and Nozaki et al. (2001). Particles transported by rivers are one of the major sources of the four naturally occurring radium isotopes in estuaries:  $^{224}\text{Ra}$  (half-life = 3.6 d),  $^{223}\text{Ra}$  (11.4 d),  $^{228}\text{Ra}$  (5.7 yr), and  $^{226}\text{Ra}$  (1,600 yr). As river water mixes with seawater, the water's ionic strength increases and the radium isotopes are released from particles by ion exchange reactions. This results in the well-documented nonconservative distribution of radium versus salinity with a maximum concentration occurring in the mixing zone (Li et al. 1977).

In this study we focused our investigation on the Chao Phraya River that flows into the upper Gulf of Thailand. We combined the application of radon and radium isotopes to estimate groundwater discharge and estuarine mixing in the Chao Phraya estuary. An earlier investigation of barium,  $^{226}\text{Ra}$ , and  $^{228}\text{Ra}$  distribution in this estuary by Nozaki et al. (2001) indicated that there could be substantial groundwater discharge in the area. Unfortunately, those investigators were unable to estimate the magnitude of SGD because they had no way of estimating the residence time of waters in the estuary–Gulf of Thailand system. In our study we measured short-lived radium isotopes to calculate the estuary–gulf exchange rates and combined this information with radon and long-lived radium isotope distributions to estimate groundwater discharge in the estuary. We will show here that groundwater discharge in this river-dominated coastal region is important, with shoreline fluxes over one order of magnitude higher than other areas of the Gulf of Thailand.

#### Study site and experiment

*Location*—Thailand has a tropical climate with wet and dry seasons influenced by the southwest monsoon and by

tropical cyclonic storms from the South China Sea (Stansfield and Garrett 1977). These monsoon patterns strongly affect the flows in the Chao Phraya (River of Kings) and its tributaries. The average annual rainfall is about 900 to 1,400 mm yr<sup>-1</sup>. The Chao Phraya is the largest river in central Thailand (Fig. 1). It empties into the Gulf of Thailand and represents approximately half of the gulf's river input. The Chao Phraya has a large influence on industrial and agricultural development in central Thailand. There has been extensive land use development over the last 40 yr in the river basin that included irrigation projects, engineering projects for salinity control, and navigation. The river flows through Bangkok and a heavily industrialized region near the estuary.

The diurnal tide in the river mouth has an amplitude of about 1 m. Because of the strong seasonality, we designed our sampling program for both dry (January) and wet (July) field programs. During our dry season sampling in January 2004 at low river discharge, we witnessed a day of unusually high water level in the river apparently caused by an abnormally high tidal surge. The water flooded the roads stopping traffic and when drained away it flushed the debris from the streets into the river. Such events probably influence both the surface and the groundwater composition and quality in the river basin aquifers.

*Sampling and analysis techniques*—The sample collection and radon surveying was done on two cruises aboard the R/V *Chula-Vijai* of Chulalongkorn University (Bangkok, Thailand). The dry season sampling took place in January 2004 at low river discharge (47 m<sup>3</sup> s<sup>-1</sup>), and the wet season sampling was done in July 2004 during a river discharge of 430 m<sup>3</sup> s<sup>-1</sup>. These discharge figures are the sum of two gauging stations on different branches of the river located at the Chao Phraya and Rama VI dams. The location of

these gauges is about 270 and 190 km upriver to prevent tidal effects, so the discharge estimates are likely somewhat low since additional surface and groundwater inputs to the lower reaches of the river are ignored. In both seasons we sampled along transects leading from the river mouth to a distance of about 48 km upriver (a low bridge prevented the ship from going farther) and approximately 42 km from the river mouth into the upper Gulf of Thailand (Fig. 1). The surveys were performed at relatively slow speed (5–7 km h<sup>-1</sup>) to ensure good spatial resolution for our automated radon measurements.

We used a multidetector continuous radon measurement system for radon mapping. The automated radon system analyzes <sup>222</sup>Rn from a constant stream of water pumped from about 1 m depth. The water passes through an air–water exchanger that distributes radon from the running flow of water to a closed air loop. The air stream is fed to a series of commercial radon-in-air monitors (RAD-7, Durrige). We used three detectors that were arranged in parallel, and they determined the concentration of <sup>222</sup>Rn by electrostatic collection and measurement of the  $\alpha$ -emitting daughter, polonium-218. Since the distribution of radon at equilibrium between the air and water phases is governed by a well-known temperature dependence, the radon concentration in the water is easily calculated. We used a protocol that provided a new reading of the <sup>222</sup>Rn concentration in the surface waters every 10 min. Our radon mapping system also incorporates integrated global positioning system navigation, depth sounding, salinity (conductivity), and temperature measurements (Burnett et al. 2001a; Dulaiova et al. 2005). We set up another RAD-7 detector on the boat to measure radon concentration in air along the transect during the cruise. We received wind speed data for the period of our study from a meteorological station of the Thai Navy in Hua Hin (the western side of the upper Gulf of Thailand).

We also measured the content and isotopic composition of dissolved radium in the river and gulf. We used MnO<sub>2</sub>-impregnated fibers to concentrate radium from large volume water samples collected along the same track as our radon survey. These fibers quantitatively adsorb radium from seawater as long as the flow rate of water passing through the fiber is maintained at a rate of less than 2 L min<sup>-1</sup> (Moore 1976). Discrete water samples from the river and offshore were collected by quickly pumping into large (>100 liter) plastic barrels and then processing measured volumes of water by slowly pumping the water through cartridges filled with ~150 cm<sup>3</sup> of MnO<sub>2</sub> fiber. We connected two cartridges in series and put raw acrylic fiber in the upstream cartridge to filter out the bulk of the suspended particles. The MnO<sub>2</sub>-coated fiber was in the downstream cartridge. The volume measurements were made using a calibrated mechanical flowmeter (Kobold, model WT-5020). Typical volumes for the radium measurements were ~100 liters.

We also collected radium on MnO<sub>2</sub> fibers by towing fibers for 30–60 min in a mesh bag behind the ship. Such samples cannot quantify the activities of Ra isotopes because there is no volume measurement, but they are useful for assessing radium activity ratios (AR). After

either collection method, the excess water was squeezed out of the fiber by hand and the fibers were sent via express courier back to our laboratories at Florida State University, where they were washed with radium-free water to remove the salt from the fibers before radium measurement. We also collected the raw acrylic fiber from the upstream cartridge containing particulate material from the more heavily loaded samples, and these were also analyzed for radium activity ratios. The <sup>223</sup>Ra and <sup>224</sup>Ra measurements were made within a few days of sampling using a specially designed delayed coincidence system (Moore and Arnold 1996). On the same system we counted thorium-228 collected on the fiber to calculate the excess <sup>224</sup>Ra values. All <sup>224</sup>Ra values indicated throughout this paper for aqueous samples are excess <sup>224</sup>Ra. The long-lived <sup>226</sup>Ra and <sup>228</sup>Ra were measured at a later date by gamma spectrometry after ashing the fiber in custom-made stainless steel crucibles and then pressing it into wafers. The samples were aged for about 3 weeks and then counted on an intrinsic germanium detector using the actinium-228 peaks at 338 and 911 keV for <sup>228</sup>Ra and the lead-214 and bismuth-214 peaks at 259, 352, and 609 keV for <sup>226</sup>Ra (Dulaiova and Burnett 2004).

We measured conductivity–temperature–depth profiles and collected surface water samples for nutrient analysis at each radium station. The temperature, salinity, and nutrient results have been presented elsewhere (Wattayakorn et al. 2004).

Groundwater wells from three locations were sampled for conductivity, radon, and radium isotope concentrations. The radon was measured using a RAD–H<sub>2</sub>O system that is basically a portable 250-mL Rn-emanation bottle attached to the RAD-7 radon-in-air detector. The radium isotopes were measured from 20-liter water samples using the MnO<sub>2</sub>-fiber technique.

We also collected several surface sediment samples in the eastern part of the Gulf of Thailand that were dried and analyzed by gamma spectrometry.

River flux measurements were made at a downstream station during the same periods as our isotopic measurements in January and July 2004 following a method developed by Kjerfve (1979). The main purpose of these measurements was to estimate the actual net river flow at a station near the mouth of the river. Hourly measurements of water current (speed and direction) together with temperature, salinity, and total suspended solids were carried out for 49 h at two sampling stations in a cross section of the Chao Phraya River 18 km upstream of the river mouth. The stations were off the east and west banks of the river at water depths of 8 and 5 m, respectively. An observation that will have important bearing on our results was that the water level at the tide gauge on 23 January 2004 at high tide was 2.55 m above mean sea level, which is 0.9 m above the predicted tide. The water levels measured in July were close to the predicted ranges.

## Results

*Horizontal surface and vertical salinity profiles*—The difference in freshwater flow during the two seasons had

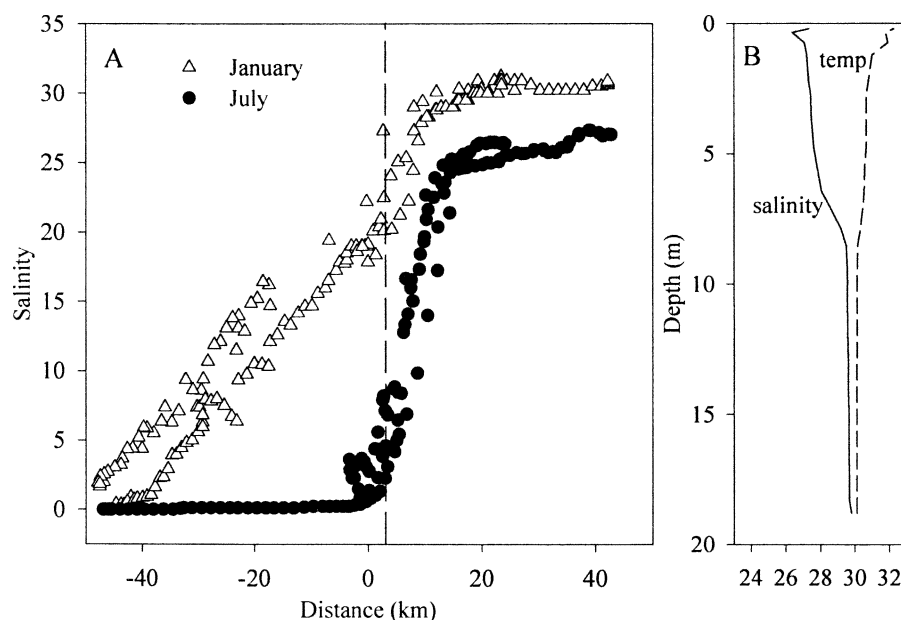


Fig. 2. (A) Horizontal salinity profile in near-surface water in the river and estuary. Zero kilometers is at the river mouth, negative distances are upriver, positive are offshore. Differences in salinity at the same location during the same survey were due to tidal effects. (B) Salinity and temperature vertical profile at the farthest offshore station (+42 km) in July showing stratification. The January profile showed the water column well mixed at approximately the same location.

a dramatic effect on the distribution of surface salinity in the river (Fig. 2A). Salt intrusion was observed more than 40 km upstream during the January sampling. In July, freshwater was found throughout the entire river and the salt wedge was pushed seaward within a few kilometers of the river mouth. At the farthest station offshore (42 km) in January we measured a salinity of 31 throughout the water column, while in July the surface waters in the same area were 27 and the bottom water 30. The gulf water was stratified in July with an 8-m thick mixed layer on the surface, while there was little to no stratification in January (Fig. 2B).

*Radon surveying*—Variations in freshwater discharge also made an impact on the concentrations of radon detected in the river. The concentrations in the river were roughly 30% lower during the high flow period in July compared with January ( $\sim 4,000$  compared with  $\sim 6,000$  dpm  $m^{-3}$ ) (Fig. 3). However, the spatial pattern of the concentrations remained much the same in the two seasons. In both surveys, the highest concentrations of  $^{222}\text{Rn}$  occurred at or just beyond the mouth of the river, and the drop-off from the high values near the river's mouth out to sea was rapid, systematic, and nearly identical. The radon activity decreased to the same level in both seasons within 10 km of the river mouth (at salinities of 25 in January and 7 in July).

The radon activity in a groundwater well (salinity  $\sim 0$ ) within  $\sim 100$  m of the mouth of the river measured by an air–water exchanger was  $376,000 \pm 70,000$  dpm  $m^{-3}$  ( $n = 6$ ) and  $372,000 \pm 48,000$  dpm  $m^{-3}$  ( $n = 1$ ) measured by a RAD–H<sub>2</sub>O system. We measured a radon concentration

of  $930,000 \pm 64,000$  dpm  $m^{-3}$  ( $n = 4$ ) also by RAD–H<sub>2</sub>O in another nearby well (also only  $\sim 100$  m from the river mouth) that had a salinity of 1.2. Still another well in the same location and depth (70 m below surface) had  $594,000 \pm 53,000$  dpm  $m^{-3}$  ( $n = 2$ ) of radon. Unfortunately, we were limited to only these “wells of opportunity” in the river mouth area, but we were able to sample waters from seepage meters and a few other wells in various locations in the eastern and western Gulf of Thailand in which radon activities ranged from 100,000 to 2,000,000 dpm  $m^{-3}$  (locations and depths listed in Table 1).

River bank well locations: W1, W2 oil factory,  $13^{\circ}36'02.50\text{N}$  and  $100^{\circ}33'38.36\text{E}$ ; W3 private house,  $13^{\circ}35'48.67\text{N}$  and  $100^{\circ}35'01.28\text{E}$ . Sri Racha well locations: SR 1,  $13^{\circ}09'20.45\text{N}$  and  $100^{\circ}55'16.43\text{E}$ ; SR 2,  $13^{\circ}09'29.12\text{N}$  and  $100^{\circ}54'56.95\text{E}$ . Hua Hin well location: HH 1,  $12^{\circ}48'51.96\text{N}$  and  $99^{\circ}59'25.92\text{E}$ . All other wells are within a few kilometers of the coast.

The atmospheric radon concentrations measured on the research vessel varied between 0 and 400 dpm  $m^{-3}$  with an average of  $180 \pm 90$  dpm  $m^{-3}$  ( $n = 60$ ).

*Dissolved radium isotopes*—The spatial distribution of dissolved radium isotopes also showed some differences with river discharge (Tables 2, 3). Although these distributions showed some seasonal variations, the dissolved radium isotope distributions plotted against salinity are similar in January and July (Fig. 4). Except for several samples that seem anomalously low in  $^{224}\text{Ra}$  activity in January, the  $^{224}\text{Ra}$ ,  $^{223}\text{Ra}$ , and  $^{226}\text{Ra}$  activities increased from a low activity at zero salinity to a peak activity between about 10 and 17 and then decreased as salinity

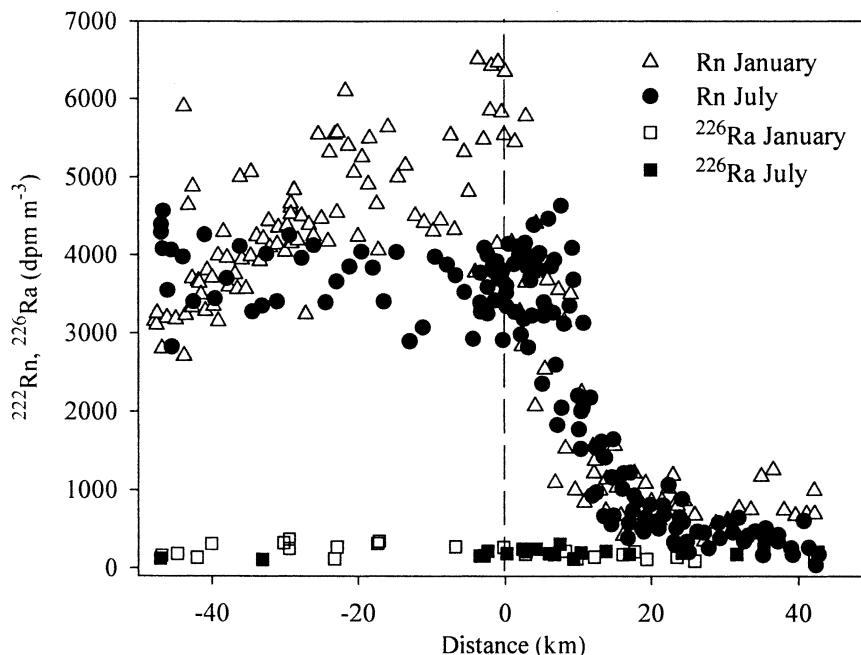


Fig. 3. Activity of  $^{222}\text{Rn}$  and its parent  $^{226}\text{Ra}$  as a function of distance in the river and Gulf of Thailand in January and July 2004.

increased further. On our transect in January, we never reached completely marine conditions or South China Sea salinities (32–33), and the short-lived radium activities did not decrease to supported thorium levels that we expected to see if our transect extended far enough into the gulf. We found that the  $^{223}\text{Ra}$  and  $^{226}\text{Ra}$  peak activities were higher in January (low flow) than July (high flow), a pattern that has been observed before for other large rivers (Moore and Krest 2004). The long-lived  $^{228}\text{Ra}$ , on the other hand, reaches maximum activity in January between salinities 25

and 31 that is at much higher salinities than the other radium isotopes. We observed a much smaller decrease in the  $^{228}\text{Ra}$  activity in July, again because our transect did not extend far enough out into the gulf to reach higher salinities. Nozaki et al. (2001) had found very similar trends of  $^{226}\text{Ra}$  and  $^{228}\text{Ra}$  versus salinity in the Chao Phraya estuary in their July and November 1996 samplings. Those investigators measured  $^{226}\text{Ra}$  activities ranging from 170 to 260  $\text{dpm m}^{-3}$  in the river and estuary, respectively, and  $^{228}\text{Ra}$  ranging from 200 to 1,100  $\text{dpm m}^{-3}$ .

Table 1. Dissolved radium isotopes and  $^{222}\text{Rn}$  activities measured in wells on land near the Gulf of Thailand coastline. The uncertainties are estimated at  $\pm 10\%$  based on counting statistics. Known depths and salinities are also indicated. Nd, no depth information. X, pore-water values obtained from surface sediments in the coastal zone, either collected from benthic chambers (S1, NC, C1) or determined by sediment equilibration (pw1, pw2). The benthic chambers and some of the wells were located in Sri Racha (SR) in the eastern Gulf of Thailand and Hua Hin (HH) in the western coastline of the gulf (Fig. 1A).

| Well       | Depth (m) | Salinity | $^{222}\text{Rn}$<br>( $\text{dpm m}^{-3}$ ) | $^{223}\text{Ra}$<br>( $\text{dpm m}^{-3}$ ) | $^{224}\text{Ra}$<br>( $\text{dpm m}^{-3}$ ) | $^{226}\text{Ra}$<br>( $\text{dpm m}^{-3}$ ) | $^{228}\text{Ra}$<br>( $\text{dpm m}^{-3}$ ) |
|------------|-----------|----------|--|--|--|--|--|
| River bank |           |          |  |  |  |  |  |
| W1         | 80        | 0        | 376,000                                      | 5.6  | 1,560  | 1,050  | 1,780  |
| W2         | 72        | 1.2      | 930,000                                      | 58   | 780  | 13,500                                       | 990  |
| W3         | 68        |          | 594,000                                      |  |  |  |  |
| SR1        | nd        | 0.4      | 255,000                                      | 10   | 820  | 380  | 460  |
| SR2        | nd        | 0.6      | 251,000                                      | 130  | 2,260  | 760  | 1,480  |
| SR S1      | X         | 31.1     |  | 40   | 490  | 440  | 380  |
| SR NC      | X         | 30.4     | 240,000                                      | 1,220  | 32,500                                       | 1,100  | 3,410  |
| SR C1      | X         | 31       |  | 270  | 8,270  | 1,920  | 2,880  |
| SR pw1     | X         |          | 885,000                                      |  |  |  |  |
| SR pw2     | X         |          | 440,000                                      |  |  |  |  |
| HH1        | 100       | 0        | 2,010,000                                    | 130  | 5,610  | 750  | 5,190  |
| HH2        | 20        | 0        | 353,000                                      |  |  |  |  |
| HH4        | 5         | 0        | 100,000                                      | 120  | 1,200  | 2,120  | 6,260  |
| HH S1      | X         |          |  | 320  | 8,680  | 390  | 2,690  |

Table 2. Ra isotope activities for discrete samples collected in the Chao Phraya River and estuary. The uncertainties are estimated at  $\pm 10\%$  based on counting statistics.

| Sample  | Salinity | Distance (km) | $^{223}\text{Ra}$ (dpm $\text{m}^{-3}$ ) | $^{224}\text{Ra}$ (dpm $\text{m}^{-3}$ ) | $^{226}\text{Ra}$ (dpm $\text{m}^{-3}$ ) | $^{228}\text{Ra}$ (dpm $\text{m}^{-3}$ ) |
|---------|----------|---------------|--|--|--|--|
| January |          |               |  |  |  |  |
| B1      | 16.2     | -17.4         | 63                                       | 400                                      | 310                                      | 950                                      |
| B2      | 13.1     | -22.8         | 57                                       | 530                                      | 270                                      | 770                                      |
| B3      | 7.4      | -30.2         | 34                                       | 680                                      | 330                                      | 600                                      |
| B4      | 4.4      | -40.0         | 21                                       | 610                                      | 310                                      | 610                                      |
| B5      | 2.0      | -46.8         | 15                                       | 340                                      | 160                                      | 310                                      |
| B6      | 0.4      | -44.7         | 8  | 200                                      | 190                                      | 240                                      |
| B7      | 0.9      | -42.1         | 9  | 190                                      | 140                                      | 200                                      |
| B8      | 8.6      | -29.4         | 54                                       | 790                                      | 250                                      | 680                                      |
| B9      | 8.6      | -29.4         | 27                                       | 720                                      | 370                                      | 960                                      |
| B10     | 11.5     | -23.2         | 19                                       | 390                                      | 120                                      | 130                                      |
| B11     | 14.7     | -17.2         | 48                                       | 290                                      | 350                                      | 930                                      |
| B12     | 19.4     | -6.9          | 50                                       | 330                                      | 270                                      | 880                                      |
| B13     | 22.2     | -0.2          | 50                                       | 470                                      | 270                                      | 1,160                                    |
| B14     | 27.3     | 2.7           | 44                                       | 700                                      | 180                                      | 950                                      |
| B15     | 29.4     | 9.7           | 33                                       | 310                                      | 120                                      | 990                                      |
| B16     | 30.2     | 17.7          | 19                                       | 250                                      | 210                                      | 1,240                                    |
| B17     | 30.2     | 25.9          | 12                                       | 140                                      | 100                                      | 790                                      |
| B18     | 30.9     | 42.2          | 12                                       | 100                                      | 140                                      | 910                                      |
| B19     | 29.0     | 8.2           | 41                                       | 580                                      | 220                                      | 1,230                                    |
| B20     | 30.1     | 12.1          | 27                                       | 230                                      | 140                                      | 980                                      |
| B21     | 30.3     | 16.1          | 22                                       | 190                                      | 180                                      | 1,070                                    |
| B22     | 30.9     | 19.4          | 20                                       | 240                                      | 120                                      | 1,190                                    |
| B23     | 31.2     | 23.5          | 11                                       | 120                                      | 140                                      | 800                                      |
| July    |          |               |  |  |  |  |
| B24     | 0.1      | -47.0         | 5  | 170                                      | 120                                      | 210                                      |
| B25     | 0.1      | -33.1         | 5  | 200                                      | 110                                      | 100                                      |
| B25dupl |          |               | 5  | 210                                      | 90                                       | 120                                      |
| B26     | 0.2      | -3.5          | 7  | 270                                      | 160                                      | 170                                      |
| B27     | 0.8      | 0.2           | 13                                       | 290                                      | 190                                      | 210                                      |
| B28     | 8.0      | 6.0           | 36                                       | 710                                      | 190                                      | 650                                      |
| B29     | 3.5      | -2.4          | 27                                       | 510                                      | 220                                      | 360                                      |
| B30     | 8.5      | 4.2           | 34                                       | 690                                      | 250                                      | 690                                      |
| B31     | 19.6     | 9.3           | 27                                       | 460                                      | 120                                      | 700                                      |
| B32     | 25.4     | 17.0          | 31                                       | 260                                      | 180                                      | 1,450                                    |
| B33     | 26.4     | 24.2          | 22                                       | 210                                      | 260                                      | 1,390                                    |
| B34     | 27.0     | 31.6          | 28                                       | 190                                      | 180                                      | 1,290                                    |
| B35     | 27.7     | 35.3          | 25                                       | 180                                      | 250                                      | 1,380                                    |
| B36     | 28.0     | 42.6          | 16                                       | 60                                       | 210                                      | 1,340                                    |
| B37     | 14.9     | 7.4           | 37                                       | 890                                      | 310                                      | 1,100                                    |
| B39     | 2.5      | -2.9          | 22                                       | 420                                      | 160                                      | 430                                      |
| B40     | 12.0     | 2.4           | 33                                       | 700                                      | 240                                      | 830                                      |
| B41     | 6.0      | 2.8           | 25                                       | 580                                      | 210                                      | 650                                      |
| B42     | 17.2     | 6.7           | 41                                       | 770                                      | 180                                      | 800                                      |
| B43     | 21.4     | 10.3          | 28                                       | 530                                      | 200                                      | 900                                      |
| B44     | 27.2     | 24.2          | 35                                       | 220                                      | 200                                      | 1,420                                    |
| B45     | 25.1     | 13.7          | 38                                       | 550                                      | 220                                      | 1,420                                    |

*Radium in suspended particles and bottom sediments*—Total suspended sediment (TSS) concentrations measured at the river mouth station ( $\sim 18$  km) varied between 4 and 121  $\text{g m}^{-3}$  with a mean of  $36 \pm 28$   $\text{g m}^{-3}$  ( $n = 50$ ) in January and ranged from 20 to 91  $\text{g m}^{-3}$  with a mean of  $42 \pm 16$   $\text{g m}^{-3}$  ( $n = 50$ ) in July (Wattayakorn et al. 2004). At Sta. B25 (33 km upstream from the river mouth) we processed duplicate water samples and we also retained the prefilter from the cartridges. The radium activity ratios measured on the suspended particles from this station (zero

salinity) collected by the raw acrylic fiber are provided in Table 4. These ratios have high uncertainties due to the low particulate mass collected on the raw fibers. The  $^{234}\text{Th}$  ( $^{238}\text{U}$ ) :  $^{235}\text{U}$  activity ratio measured by gamma spectrometry on these particles is  $\sim 22$ , nearly identical to the natural abundance ratio of 21.7 expected from the  $^{238}\text{U}$  :  $^{235}\text{U}$  natural decay chains. The short-lived radium isotopes were counted via a delayed coincidence counting system (Moore and Arnold 1996; Sun and Torgersen 2001) and thus likely represent only the radium attached to particle surfaces. The

Table 3. Ra isotopes on the towed fibers. The uncertainties are estimated at  $\pm 10\%$  based on counting statistics.

| Sample  | Salinity | Distance (km) | $^{223}\text{Ra}$ (dpm fiber $^{-1}$ ) | $^{224}\text{Ra}$ (dpm fiber $^{-1}$ ) | $^{226}\text{Ra}$ (dpm fiber $^{-1}$ ) | $^{228}\text{Ra}$ (dpm fiber $^{-1}$ ) |
|---------|----------|---------------|--|--|--|--|
| January |          |               |  |  |  |  |
| CV1     | 14.0     | -18.8         | 3.2                                    | 43                                     | 39                                     | 112                                    |
| CV2     | 12.9     | -22.5         | 2.2                                    | 33                                     | 19                                     | 58                                     |
| CV3     | 9.6      | -25.8         | 1.4                                    | 21                                     | 11                                     | 14                                     |
| CV4     | 8.0      | -29.1         | 1.2                                    | 27                                     | 13                                     | 13                                     |
| CV5     | 6.4      | -33.1         | 2.3                                    | 33                                     | 23                                     | 30                                     |
| CV6     | 5.6      | -36.7         | 0.8                                    | 21                                     | 12                                     | 15                                     |
| CV7     | 3.8      | -40.5         | 1.1                                    | 13                                     | 20                                     | 12                                     |
| CV8     | 2.4      | -43.9         | 0.5                                    | 9                                      | 11                                     | 13                                     |
| CV9     | 1.7      | -47.5         | 0.4                                    | 5                                      | nd                                     | nd                                     |
| CV10    | 0.7      | -42.8         | 1.1                                    | 13                                     | 22                                     | 16                                     |
| CV11    | 1.6      | -39.9         | 1.5                                    | 23                                     | 13                                     | 21                                     |
| CV12    | 3.5      | -35.9         | 0.6                                    | 19                                     | 6                                      | 6                                      |
| CV13    | 6.2      | -31.5         | 1.0                                    | 23                                     | 6                                      | 18                                     |
| CV14    | 7.6      | -26.6         | 1.5                                    | 29                                     | 11                                     | 20                                     |
| CV15    | 10.8     | -21.5         | 2.0                                    | 47                                     | 21                                     | 52                                     |
| CV16    | 14.3     | -14.7         | 3.4                                    | 16                                     | 33                                     | 103                                    |
| CV17    | 17.1     | -7.0          | 5.2                                    | 69                                     | 17                                     | 55                                     |
| CV18    | 19.1     | -0.7          | 5.2                                    | 81                                     | 21                                     | 86                                     |
| CV19    | 24.4     | 2.4           | 5.0                                    | 74                                     | 17                                     | 110                                    |
| CV20    | 26.9     | 10.8          | 1.9                                    | 22                                     | 9                                      | 73                                     |
| CV21    | 27.5     | 18.6          | 2.8                                    | 28                                     | 15                                     | 138                                    |
| CV22    | 27.6     | 27.7          | 6.4                                    | 34                                     | 19                                     | 187                                    |
| CV23    | 28.3     | 38.5          | 1.9                                    | 21                                     | 18                                     | 152                                    |
| CV24    | 27.2     | 10.1          | 2.7                                    | 37                                     | 21                                     | 145                                    |
| CV25    | 27.9     | 14.0          | 4.8                                    | 28                                     | 18                                     | 106                                    |
| CV26    | 27.9     | 30.5          | 2.3                                    | 34                                     | 39                                     | 251                                    |
| July    |          |               |  |  |  |  |
| CV27    | 0.1      | -46.5         | 0.3                                    | 6                                      | 8                                      | 8                                      |
| CV28    | 0.1      | -48.8         | 0.6                                    | 7                                      | 6                                      | 7                                      |
| CV29    | 0.1      | -32.8         | 0.1                                    | 7                                      | 2                                      | 6                                      |
| CV30    | 0.1      | -21.9         | 0.5                                    | 7                                      | 3                                      | 3                                      |
| CV31    | 0.1      | -10.5         | 0.4                                    | 9                                      | 3                                      | 3                                      |
| CV32    | 0.2      | -3.5          | 0.6                                    | 9                                      | 10                                     | 5                                      |
| CV33    | 0.3      | 1.9           | 0.9                                    | 32                                     | 16                                     | 26                                     |
| CV34    | 5.1      | 5.8           | 2.4                                    | 47                                     | 25                                     | 51                                     |
| CV35    | 2.4      | 0.3           | 1.2                                    | 23                                     | 16                                     | 16                                     |
| CV36    | 3.5      | -0.7          | 0.8                                    | 20                                     | 17                                     | 25                                     |
| CV37    | 10.7     | 6.2           | 0.6                                    | 11                                     | 10                                     | 16                                     |
| CV38    | 18.7     | 10.6          | 0.9                                    | 9                                      | 12                                     | 21                                     |
| CV39    | 22.8     | 16.7          | 1.8                                    | 13                                     | 17                                     | 58                                     |
| CV40    | 23.6     | 23.6          | 2.5                                    | 13                                     | 27                                     | 106                                    |
| CV41    | 24.2     | 31.6          | 1.4                                    | 11                                     | 21                                     | 96                                     |
| CV42    | 25.0     | 38.1          | 2.5                                    | 10                                     | 35                                     | 167                                    |
| CV43    | 24.8     | 38.5          | 6.3                                    | 29                                     | 55                                     | 331                                    |
| CV44    | 23.7     | 25.7          | 4.3                                    | 26                                     | 40                                     | 196                                    |
| CV45    | 18.9     | 11.9          | 2.0                                    | 56                                     | 15                                     | 41                                     |
| CV46    | 5.6      | 3.2           | 3.9                                    | 89                                     | 47                                     | 79                                     |
| CV47    | 4.6      | 0.5           | 2.2                                    | 41                                     | 24                                     | 36                                     |
| CV48    | 10.7     | 5.2           | 1.9                                    | 34                                     | 20                                     | 50                                     |
| CV49    | 17.9     | 9.4           | 4.4                                    | 96                                     | 43                                     | 131                                    |
| CV50    | 22.5     | 13.3          | 3.2                                    | 34                                     | 21                                     | 118                                    |
| CV51    | 24.6     | 20.8          | 0.9                                    | 9                                      | 13                                     | 56                                     |
| CV52    | 24.4     | 19.9          | 3.1                                    | 46                                     | 46                                     | 243                                    |
| CV53    | 20.3     | 13.4          | 4.5                                    | 47                                     | 34                                     | 121                                    |
| CV54    | 7.0      | 6.3           | 2.3                                    | 55                                     | 26                                     | 62                                     |
| CV55    | 0.5      | -0.3          | 0.4                                    | 18                                     | 18                                     | 30                                     |

Nd, not determined.

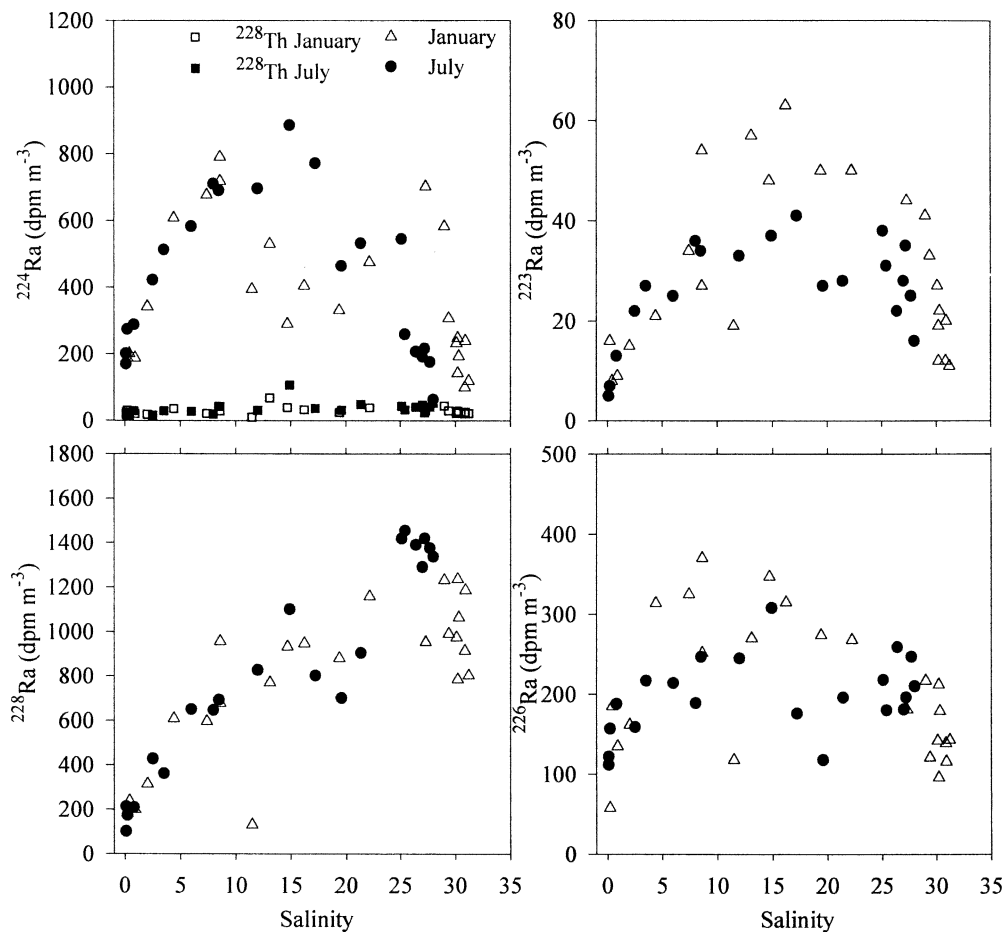


Fig. 4. Radium isotope distributions in discrete samples of surface water plotted against salinity in the Chao Phraya River and offshore in January and July 2004.

$^{226}\text{Ra} : ^{223}\text{Ra}$  activity ratio is also very close to the natural abundance ratio both on the particles and in the river ( $\text{AR} = 18 \pm 5$ ). The other isotopic activity ratios on the particles and dissolved in the water agree within the estimated

Table 4. Radium activity ratios measured in zero-salinity water at Sta. B25 located  $-33$  km upstream in the Chao Phraya River. The particles were collected on a  $0.45\text{-}\mu\text{m}$  cartridge-type filter, and the river water values are the average of the B25 samples collected in duplicate. The short-lived  $^{223}\text{Ra}$  and  $^{224}\text{Ra}$  were measured on the delayed coincidence counter, and the values measured probably represent only the adsorbed radium concentrations. The long-lived  $^{226}\text{Ra}$  and  $^{228}\text{Ra}$  were measured by gamma spectrometry, and the concentrations are the total radium present in the particles. The short- to long-lived radium ratios on the particles are thus only approximate. Uncertainties represent  $\pm 1 \sigma$  based on counting statistics.

|                                     | Particles       | River water     |
|-------------------------------------|-----------------|-----------------|
| $^{226}\text{Ra} : ^{228}\text{Ra}$ | $0.85 \pm 0.11$ | $0.87 \pm 0.21$ |
| $^{224}\text{Ra} : ^{228}\text{Ra}$ | $0.67 \pm 0.28$ | $1.78 \pm 0.31$ |
| $^{224}\text{Ra} : ^{223}\text{Ra}$ | $27 \pm 17$     | $37 \pm 4$      |
| $^{226}\text{Ra} : ^{223}\text{Ra}$ | $18 \pm 9$      | $18 \pm 5$      |
| $^{234}\text{Th} : ^{235}\text{U}$  | $22 \pm 5$      | nd              |

Nd, not determined.

uncertainties. One exception is the  $^{224}\text{Ra} : ^{228}\text{Ra}$  AR, which is much higher in the dissolved state in the river water ( $^{224}\text{Ra}$  in excess of  $^{228}\text{Th}$ ) than on the particles (total  $^{224}\text{Ra}$ ). We were not able to calculate the specific radium isotope activities on these samples because the prefilters were not preweighed, the radon-emanation coefficients from these particles are unknown, and there was evidence of particulate losses from the fibers during sample handling. However, we were able to estimate the particulate radium isotope activities from one river water sample that we passed through a  $0.45\text{-}\mu\text{m}$  filter. During the July sampling at the same station (B25), we passed 11.5 liters of water through a cartridge-type filter and measured the radium activity on the particles that it collected. Based on the water volume and assuming that the average TSS value ( $42 \text{ g m}^{-3}$ ) was applicable to this sample, we estimated the  $^{226}\text{Ra}$  specific activity on the suspended sediments at about  $5 \text{ dpm g}^{-1}$ .

The results of gamma-spectrometric analysis of sediments collected in the eastern part of Gulf of Thailand are listed in Table 5. At this location the sediments are constantly exposed to salty seawater with high ionic strength (salinity  $\sim 32$ ) and thus should have lost their desorbable radium activity. Radium isotopes were also

Table 5. Gamma-spectrometric results of sediments from the eastern shore (Sri Racha) of the upper Gulf of Thailand. Uncertainties represent  $\pm 1 \sigma$  based on counting statistics.

| Sediment  | $^{226}\text{Ra}$<br>(dpm g <sup>-1</sup> ) | $^{228}\text{Ra}$<br>(dpm g <sup>-1</sup> ) | $^{234}\text{Th}$<br>(dpm g <sup>-1</sup> ) | $^{235}\text{U}$<br>(dpm g <sup>-1</sup> ) |
|-----------|---|---|---|--|
| Silty     | 5.4 $\pm$ 0.6                               | 4.3 $\pm$ 0.7                               | 4.7 $\pm$ 1.0                               | 0.4 $\pm$ 0.1                              |
| Sand/silt | 3.5 $\pm$ 0.2                               | 3.4 $\pm$ 0.4                               | 5.9 $\pm$ 1.1                               | 0.9 $\pm$ 0.2                              |
| Sandy     | 2.0 $\pm$ 0.1                               | 1.7 $\pm$ 0.1                               | 3.2 $\pm$ 0.4                               | 0.2 $\pm$ 0.1                              |

measured in several groundwater wells in the region (Table 1).

## Discussion

*Isotopic trends*—High radon concentrations in the river and river mouth decrease toward supported levels offshore. This reduction in the radon concentration in the offshore direction is due to a combination of mixing with low activity waters offshore, radioactive decay, and emanation of radon into the atmosphere. Unlike radon, the distribution of radium isotopes is expected to be strongly influenced by salinity because the salt content governs ion exchange reactions that result in release of radium adsorbed onto particle surfaces (Li et al. 1977; Moore et al. 1995). When radium isotopes measured in the discrete samples are plotted against salinity, the concentrations are more comparable than those plotted against geographic position (Fig. 4). There was an unusual distribution of  $^{224}\text{Ra}$  (excess) during the January sampling expressed as an apparent double peak at salinities 10 and 27 with a low point at 15 (15 km upstream). One would expect a similar trend of  $^{224}\text{Ra}$  versus salinity in both sampling periods as observed for the other radium isotopes. However, in January the downstream river flux measurements obtained using the Kjerfve (1979) method indicated a much higher apparent discharge (281 m<sup>3</sup> s<sup>-1</sup>) relative to the gauged values upstream (47 m<sup>3</sup> s<sup>-1</sup>). The net river flux calculated for July (324 m<sup>3</sup> s<sup>-1</sup>) at that time was much closer to the gauged values (430 m<sup>3</sup> s<sup>-1</sup>) at that time. We interpret the apparent high water-flux values in January and the low  $^{224}\text{Ra}$  values as being due to a tidal surge of gulf water entering the lower reaches of the river. The “flux station” results indicated that there was a higher than usual water level (water levels about 0.9 m above predicted tidal stage) and current velocity on 23 January 2004 (our sampling dates were 23 to 25 January 2004). This surge was apparently caused by a high pressure front passing through the South China Sea and pushing seawater into the gulf and consequently into the lower reaches of the river. We think that the low  $^{224}\text{Ra}$  at about a salinity of 15 is a reflection of gulf water brought into the river during this event. The short duration of this surge would explain why only the radium isotope with the shortest half-life was affected. The surge could also be a reason why the radon distribution in January shows a similar double peak, since  $^{224}\text{Ra}$  and the area of maximum radon activity is more landward than during our July sampling when no such surge occurred

(Fig. 3). The similarity in the  $^{222}\text{Rn}$  and  $^{224}\text{Ra}$  horizontal profiles can be explained by the fact that they likely have similar sources and the half-life of  $^{222}\text{Rn}$  (3.8 d) is very close to that of  $^{224}\text{Ra}$  (3.6 d).

The distribution of  $^{228}\text{Ra}$  and  $^{226}\text{Ra}$  plotted against salinity in both seasons revealed a different pattern than the shorter-lived radium isotopes (Fig. 4). In January, the long-lived radium isotope distributions showed a peak at about 27–28, and in July the activities increased throughout the sampled salinity range (ended at 27). This is due to the much longer half-lives of these nuclides compared to  $^{223}\text{Ra}$  and  $^{224}\text{Ra}$ .

Owing to the nonconservative distribution of radium isotopes against salinity, the activity ratios of the various radium isotopes may provide better information about possible input sources than the absolute activities. Plots of  $^{224}\text{Ra} : ^{223}\text{Ra}$  against  $^{224}\text{Ra} : ^{226}\text{Ra}$  and  $^{224}\text{Ra} : ^{223}\text{Ra}$  versus  $^{222}\text{Rn}$  measured in the discrete samples indicate that there are at least three distinctive water masses with different isotopic signatures (Fig. 5). After examining the location of the samples in these groups it is clear that the samples originate from (1) river water with high  $^{224}\text{Ra} : ^{223}\text{Ra}$  ratios and high radon concentrations; (2) Gulf of Thailand water with very low  $^{224}\text{Ra} : ^{223}\text{Ra}$  and  $^{224}\text{Ra} : ^{226}\text{Ra}$  ratios and very low radon activities; and (3) samples collected between +0 and +10 km on the transect with intermediate  $^{224}\text{Ra} : ^{223}\text{Ra}$ , high  $^{224}\text{Ra} : ^{226}\text{Ra}$  activity ratios, and the highest radon concentrations.

The  $^{224}\text{Ra} : ^{223}\text{Ra}$  ratios in group 1 are lower in January (average  $27 \pm 3$ ,  $n = 4$ ) than in July (average  $37 \pm 3$ ,  $n = 3$ ). If the particles in the river originate in the same drainage area in both seasons, we would expect these ratios to be similar. The reason why we see lower river  $^{224}\text{Ra} : ^{223}\text{Ra}$  ratios in January might be that we were not able to collect samples in zero-salinity river water that month. Radon concentrations are the highest in group 3, which represents samples from the intertidal zone called the Bangkok Bar (0 to +10 km on our transect). In this area the water depth is 5–10 m in the boat channel and only 1–2 m on either side in the intertidal zone. Our trajectory led through waters generally about 3 m deep. High radon concentrations in this area can be supported by diffusion from sediments, sediment resuspension, groundwater discharge, or a mixture of these processes.

Radium isotopes, whether from sediment resuspension or by groundwater discharge in the intertidal zone, might come from a shoal area at 1–7 km created by particle deposition. Such particles were at some point exposed to salty water and presumably lost desorbable radium. Newly deposited sediments are thus depleted in radium. However, as the sediments age the radium isotopes are regenerated by radioactive ingrowth from their thorium parents. The isotopes  $^{224}\text{Ra}$  and  $^{223}\text{Ra}$  are regenerated on the timescale of days,  $^{228}\text{Ra}$  in a few years, while  $^{226}\text{Ra}$  ingrowth is very slow, requiring thousands of years for significant ingrowth. Therefore any radium added to the system from benthic sources in this area would be relatively high in short-lived isotopes, with some  $^{228}\text{Ra}$  but not a significant source of  $^{226}\text{Ra}$ . The parent–daughter pairs of radium isotopes and their regeneration time to 99% equilibrium with their

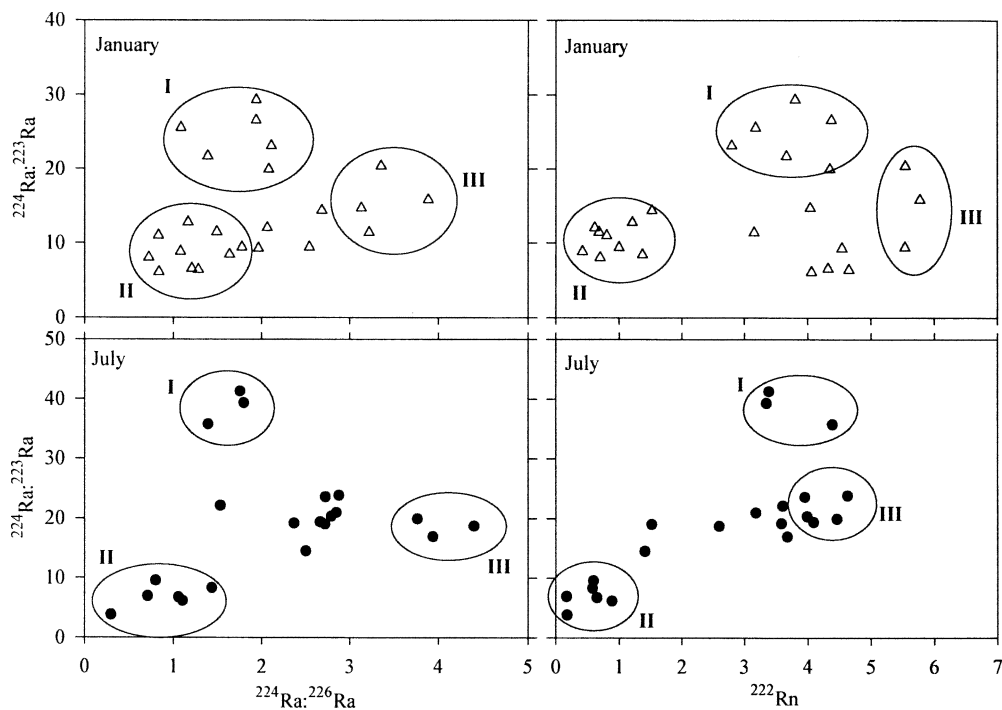


Fig. 5. Activity ratios  $^{224}\text{Ra} : ^{223}\text{Ra}$  plotted against  $^{224}\text{Ra} : ^{226}\text{Ra}$  and  $^{222}\text{Rn}$  for January and July. The three groups represent samples collected in (1) the river, (2) offshore, (3) intertidal zone.

respective parents on particles are indicated in Table 6. These calculations assume that Th isotopes are also adsorbed onto the particle surfaces.

*Estuarine radium ages*—The radium isotopic activity ratios in the estuary may give a measure of the time elapsed since the water first became enriched in radium isotopes assuming no further additions occur (Moore 2000). When radium isotopes desorb from the particles in the mixing zone, they stop being supported by their parent radionuclides. Assuming that the radium enters into the coastal waters with a constant isotopic composition at least over a period comparable to the effective mean life of the  $^{224}\text{Ra} : ^{223}\text{Ra}$  activity ratio (7.8 d), one can estimate radium ages of the water. Apparent radium ages may also be calculated using the short-lived radium isotope normalized to a long-lived isotope to compensate for dilution. Based on the  $^{224}\text{Ra} : ^{223}\text{Ra}$  activity ratio, one may use the following equation (Moore 2000):

$$\left[ \frac{^{224}\text{Ra}}{^{223}\text{Ra}} \right]_{\text{obs}} = \left[ \frac{^{224}\text{Ra}}{^{223}\text{Ra}} \right]_i \frac{e^{-\lambda_{224}t}}{e^{-\lambda_{223}t}} \quad (1)$$

where  $[^{224}\text{Ra}/^{223}\text{Ra}]_{\text{obs}}$  and  $[^{224}\text{Ra}/^{223}\text{Ra}]_i$  represent the observed and initial activity ratios of the radium source water for each data set, and  $\lambda_{224}$  and  $\lambda_{223}$  are the decay constants of  $^{224}\text{Ra}$  and  $^{223}\text{Ra}$ , respectively. For the age calculations we used the  $[^{224}\text{Ra} : ^{223}\text{Ra}]_i$  ratio of 37 for both sampling periods as explained earlier.

Solving for  $t$ , Eq. 1 becomes

$$\text{Ra age} = \ln \left[ \frac{[^{224}\text{Ra}/^{223}\text{Ra}]_i}{[^{224}\text{Ra}/^{223}\text{Ra}]_{\text{obs}}} \right] \frac{1}{\lambda_{224} - \lambda_{223}} \quad (2)$$

This method also assumes that the offshore Gulf of Thailand waters do not contain excess  $^{224}\text{Ra}$  and  $^{223}\text{Ra}$ , which should be a valid assumption since there would be no sources of these isotopes in the open gulf. Another assumption is that there are no other inputs of these isotopes to the system, which would be the case at least in July when the water was stratified and also because we sampled the surface waters in both seasons. The same approach can be applied for the ratio of  $^{224}\text{Ra}$  and long-lived isotope  $^{228}\text{Ra}$ . The measured  $^{228}\text{Ra}$  values in the estuary have to be corrected by the South China Sea ( $160 \text{ dpm m}^{-3}$ ; Nozaki 2001) levels to get  $\text{ex}^{228}\text{Ra}$ . Since the thorium-series isotopes ( $^{224}\text{Ra}$  and  $^{228}\text{Ra}$ ) are much

Table 6. The Ra isotope regeneration time on particles to 99% of the desorbable activity.

| Parent–daughter                     | Regeneration time |
|-------------------------------------|-------------------|
| $^{228}\text{Th} - ^{224}\text{Ra}$ | 22 d              |
| $^{227}\text{Th} - ^{223}\text{Ra}$ | 73 d              |
| $^{230}\text{Th} - ^{226}\text{Ra}$ | 8,000 yr          |
| $^{232}\text{Th} - ^{228}\text{Ra}$ | 37 yr             |

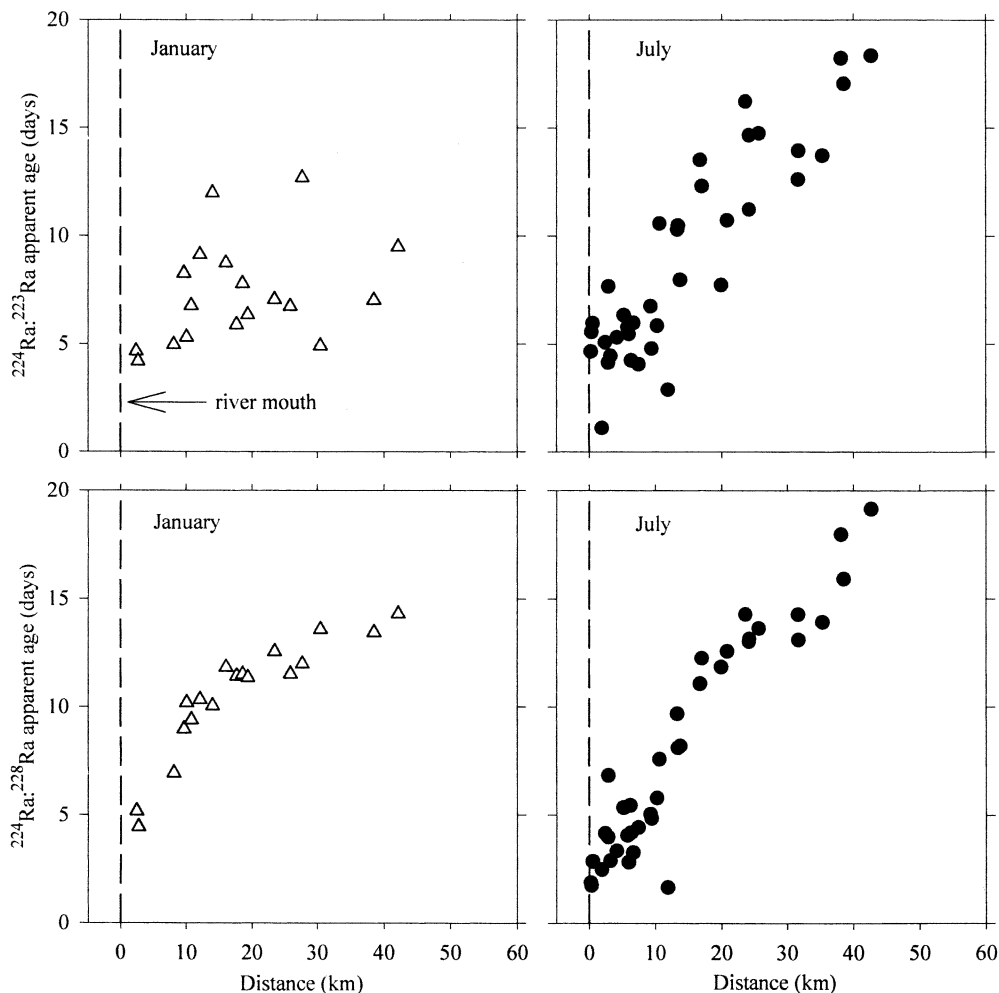


Fig. 6. Apparent radium ages of water in the Chao Phraya estuary calculated using  $^{224}\text{Ra} : ^{223}\text{Ra}$  and  $^{224}\text{Ra} : ^{228}\text{Ra}$  activity ratios for January and July 2004.

more abundant in the coastal waters off Thailand than the uranium-series isotopes ( $^{223}\text{Ra}$  and  $^{226}\text{Ra}$ ), estimating radium ages based on the  $^{224}\text{Ra} : \text{ex}^{228}\text{Ra}$  activity ratios could be more precise, at least in terms of the analytical uncertainties. We have calculated ages based on these ratios with  $[\frac{^{224}\text{Ra}}{^{228}\text{Ra}}]_i$  AR of 2.0 (based on analyses of zero-salinity river water).  $^{228}\text{Ra}$  has a half-life of 5.7 yr, which is long with respect to the half-life of  $^{224}\text{Ra}$  as well as the mixing time of nearshore waters, so we may neglect decay of  $\text{ex}^{228}\text{Ra}$ :

$$\text{Ra age} = \ln \frac{\left[ \frac{^{224}\text{Ra}}{^{228}\text{Ra}} \right]_i}{\left[ \frac{^{224}\text{Ra}}{\text{ex}^{228}\text{Ra}} \right]_{\text{obs}}} \frac{1}{\lambda_{224}} \quad (3)$$

Ages calculated by both approaches resulted in very good agreement. The calculated apparent radium ages were plotted against distance to examine possible relationships between position offshore and transport time (Fig. 6A,B). The trends and calculated ages are very similar for both isotope ratios and during both samplings, but the age

versus distance trends show more inflections in January than the smooth trends in July. There is a clear linear relationship between radium ages and distance offshore for both isotope pairs in July. The lack of a clear pattern in January is likely related to the lack of a well-defined pycnocline as well as the tidal surge event that was hypothesized based on the unusual tidal range and the river flux data.

The distribution of  $^{224}\text{Ra}$  and  $^{228}\text{Ra}$  activities against distance is shown in Fig. 7. The main dissimilarity in the offshore trends for both seasons occurs because of the much shorter half-life of  $^{224}\text{Ra}$ . This short-lived isotope decays much faster than  $^{228}\text{Ra}$ , and its concentration decreases more rapidly with distance offshore than that of the longer-lived  $^{228}\text{Ra}$ . The offshore section of  $^{228}\text{Ra}$  concentrations has a decreasing trend because of mixing with offshore waters. The inshore section of the January values is very scattered, but both the January and July data sets offshore of the river mouth indicate that no additional inputs were evident. These offshore trends support our assumptions for the age calculation model. The age calculations are supported also by the fact that both

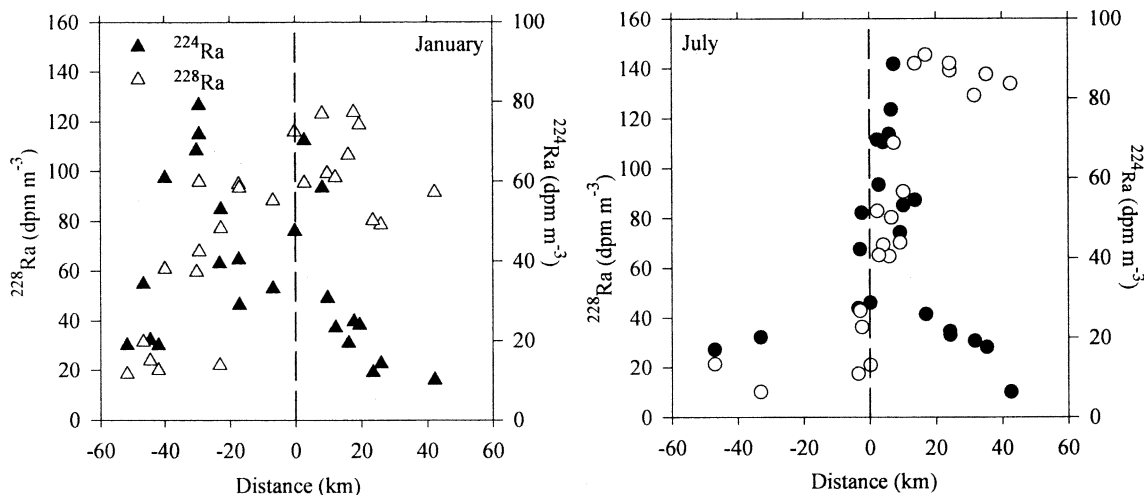


Fig. 7. Concentrations of  $^{224}\text{Ra}$  and  $^{228}\text{Ra}$  plotted against distance in the river and offshore in January and July 2004.

approaches (using  $^{224}\text{Ra} : ^{223}\text{Ra}$  and  $^{224}\text{Ra} : ^{228}\text{Ra}$ ) result in very good agreement. Overall, we can conclude based on this analysis that the apparent ages offshore are similar in both seasons and the residence time of the water in the inner shelf out to  $\sim 40$  km offshore is approximately 2 weeks.

Mixing within an estuary has the potential to distort ages calculated in this manner because of possible additional radium inputs and mixing of water masses with different histories. Indeed, the age versus distance patterns for both the dry and wet season samplings are much more complex within the mixing zones of the Chao Phraya. The salinity transition is almost entirely within the river during January, while there is a sharp salinity front right around the river mouth in July (Fig. 2). Our calculated radium ages reflect this with higher than 0 ages around the river mouth in January (Fig. 6). The pattern is systematic beyond the river mouth out toward the inner shelf.

*Estimate of SGD based on a mixing model*—The radon concentration in the river measured during our surveys ( $3,000$ – $6,000$   $\text{dpm m}^{-3}$ ) was much higher than can be supported by its parent  $^{226}\text{Ra}$ , which ranged from  $100$  to  $350$   $\text{dpm m}^{-3}$  as dissolved and  $\sim 200$   $\text{dpm m}^{-3}$  in suspended particles. The maximum total radon activity supported by its parent in the river water column is therefore about  $550$   $\text{dpm m}^{-3}$ . Additional radon sources may include diffusion from sediments, resuspension, and groundwater inputs. The amount of radon diffusing from the bottom sediments can be estimated from an experimentally defined relationship between  $^{226}\text{Ra}$  content of sediments and the corresponding measured  $^{222}\text{Rn}$  flux by diffusion (Burnett et al. 2003). That empirical relationship is based on experimental data from several different environments (both marine and fresh), where

$$\text{Flux}(\text{dpm m}^{-2} \text{d}^{-1}) = 495 \times ^{226}\text{Ra conc.} + 18.2 \quad (4)$$

From gamma-spectrometric analysis of suspended particles in the river (zero salinity), we estimate that the

bottom sediment  $^{226}\text{Ra}$  activity in the river is  $\sim 5$   $\text{dpm g}^{-1}$ . We take this as a maximum activity that may actually be lower in much of the river because most sediment would have been exposed to saline water at low river discharge during the dry season. As an estimate of  $^{226}\text{Ra}$  activity in the shallow intertidal zone we used the average activity measured in sediments collected in the coastal area of the Gulf of Thailand (Table 5;  $3.5$   $\text{dpm g}^{-1}$ ). This activity may be lower than the activity in the river bottom because it is certain that these sediments were exposed to saline water and must have lost any desorbable  $^{226}\text{Ra}$ . Radon diffusion calculated from Eq. 4 from river bottom sediment ( $5$   $\text{dpm g}^{-1}$ ) would be about  $2,500$   $\text{dpm m}^{-2} \text{d}^{-1}$ , and the diffusion from sediments in the intertidal zone is estimated at  $1,800$   $\text{dpm m}^{-2} \text{d}^{-1}$ . Assuming a steady-state system, the radon flux can also be expressed as  $\text{Flux} = \text{Rn Inventory} \times \lambda_{\text{Rn}}$ , from which the radon inventory supported by diffusion equals  $2,500$   $\text{dpm m}^{-2} \text{d}^{-1} / 0.1824 \text{d}^{-1} = 13,600$   $\text{dpm m}^{-2}$  in the river and analogously  $9,600$   $\text{dpm m}^{-2}$  in the intertidal zone. We convert the inventory into concentration by dividing by the water depth, which is  $8$  m on average in the river and only  $3$  m in the intertidal zone. The corresponding maximum  $^{222}\text{Rn}$  concentrations that can be supported by diffusion from the sediments are thus  $1,700$   $\text{dpm m}^{-3}$  in the river and  $3,000$   $\text{dpm m}^{-3}$  in the intertidal zone. Radon concentration supported by  $^{226}\text{Ra}$  in the water column and by diffusion from sediments totals to a maximum of  $2,000$   $\text{dpm m}^{-3}$  and  $3,400$   $\text{dpm m}^{-3}$  in the river and in the intertidal zone, respectively. We observed activities as high as  $5,000$ – $6,000$   $\text{dpm m}^{-3}$ , which could be corrected further for losses by atmospheric evasion and radioactive decay. We estimated radon losses via evasion to the atmosphere based on the wind, water temperature, and radon-in-air concentrations measured during the survey (Macintyre et al. 1995). In January these losses represented about  $8\%$  and in July  $6\%$  of the radon inventory in the water. The radon activities in the estuary were corrected for atmospheric evasion and also decay corrected based on the apparent radium ages of the water. The corrected radon concentra-

tions in the river and estuary were thus as high as 7,600 dpm m<sup>-3</sup>, much higher than can be accounted for by diffusion and <sup>226</sup>Ra.

We suspected that the excess radon concentrations near the mouth of the Chao Phraya could be a reflection of enhanced groundwater seepage in this area. It is very likely that groundwater in this topographically very low region has a significant saline component, i.e., recirculated Gulf of Thailand water. Any fresh groundwater flow would be directed down gradient along topographic contours and thus would tend to be concentrated toward the central axis of the river valley. The highest radon concentrations in our surveys were consistently in the central axis of the river at or just beyond its mouth.

Based on the information in Fig. 5 that identifies the groups most influenced by the different sources of radon and radium isotopes, we are able to estimate the fraction of groundwater discharge into the river and estuary. In addition to the corrections for atmospheric evasion and decay of <sup>222</sup>Rn mentioned above, we applied a decay correction to the measured <sup>224</sup>Ra : <sup>223</sup>Ra AR in the estuary using the apparent radium ages of the water. The adjusted radon concentrations and decay-corrected <sup>224</sup>Ra : <sup>223</sup>Ra AR signatures in the estuary can be combined into a three end-member mixing model:

$$\begin{aligned}
 f_O + f_R + f_{GD} &= 1, \\
 f_O^{222}\text{Rn}_O + f_R^{222}\text{Rn}_R + f_{GD}^{222}\text{Rn}_{GD} &=^{222}\text{Rn}_M, \\
 \frac{f_O^{224}\text{Ra}_O + f_R^{224}\text{Ra}_R + f_{GD}^{224}\text{Ra}_{GD} (1 - e^{-S_M/S_{Des}})}{f_O^{223}\text{Ra}_O + f_R^{223}\text{Ra}_R + f_{GD}^{223}\text{Ra}_{GD} (1 - e^{-S_M/S_{Des}})} &= \frac{^{224}\text{Ra}_M}{^{223}\text{Ra}_M} \quad (5)
 \end{aligned}$$

where  $f$  is the fraction of ocean (O), river (R), or groundwater discharge (GD) end members; <sup>222</sup>Rn<sub>O</sub>, <sup>224</sup>Ra<sub>O</sub>, and <sup>223</sup>Ra<sub>O</sub> represent radon and radium activities in the ocean end member; <sup>222</sup>Rn<sub>R</sub>, <sup>224</sup>Ra<sub>R</sub>, and <sup>223</sup>Ra<sub>R</sub> are the radon and radium activities in the river end member at zero salinity; <sup>222</sup>Rn<sub>GD</sub>, <sup>224</sup>Ra<sub>GD</sub>, and <sup>223</sup>Ra<sub>GD</sub> are identified as the radon and radium activities in the groundwater end member; and <sup>222</sup>Rn<sub>M</sub> and <sup>224</sup>Ra<sub>M</sub>/<sup>223</sup>Ra<sub>M</sub> represent the radon corrected for decay and atmospheric losses and decay-corrected radium activities measured in individual samples.

The dissolved <sup>224</sup>Ra activity (analogously the <sup>223</sup>Ra) in the river represents the sum of <sup>224</sup>Ra<sub>R</sub> and <sup>224</sup>Ra desorbed from the particles in the river as they encounter saline water. The activity due to desorption is a function of the desorbable radium activity on the particles (<sup>224</sup>Ra<sub>Des</sub>) and salinity (Krest et al. 1999; Kelly and Moran 2002). The term  $S_M$  in Eq. 5 is the measured salinity, and  $S_{Des}$  is the salinity at which the desorbable radium activity on river sediments reduces to  $e^{-1}$  of its original value. We assumed 99% radium desorption at salinity of 17 (Fig. 4); therefore, the calculated  $S_{Des}$  is 3.7. We estimated <sup>224</sup>Ra<sub>Des</sub> at about 60 dpm m<sup>-3</sup> and <sup>223</sup>Ra<sub>Des</sub> at 1.6 dpm m<sup>-3</sup> based on our measurements of radium activity differences between particles collected in the river and in the Gulf of Thailand.

The calculated radon from diffusion from the bottom sediments plus supported <sup>222</sup>Rn activity in the freshwater end member of the river is 2,000 dpm m<sup>-3</sup> (3,400 in the intertidal zone), and the river values for <sup>224</sup>Ra are 200 ± 60 dpm m<sup>-3</sup> ( $n = 4$ ) and for <sup>223</sup>Ra are 1.0 ± 1.0 dpm m<sup>-3</sup> ( $n = 4$ ) in January and for <sup>224</sup>Ra are 200 ± 60 dpm m<sup>-3</sup> ( $n = 5$ ) and for <sup>223</sup>Ra are 5.4 ± 1.0 dpm m<sup>-3</sup> ( $n = 5$ ) in July. The ocean end-member radon equals 80 dpm m<sup>-3</sup> (South China Sea <sup>226</sup>Ra activity; Nozaki et al. 2001), and the ocean end-member <sup>224</sup>Ra is 30 dpm m<sup>-3</sup> and <sup>223</sup>Ra is 7 dpm m<sup>-3</sup> for both seasons. The estimated groundwater <sup>224</sup>Ra is 800 ± 80 dpm m<sup>-3</sup> and <sup>223</sup>Ra is 60 ± 6 dpm m<sup>-3</sup> for both seasons based on measurements from a well near the estuary.

A good estimate for the groundwater end-member radon concentration is more difficult. Although groundwater radon concentrations could be estimated from values measured in the surrounding wells (Table 1), wells sampled closest to the river had very different radon activities ranging from 370,000 to 930,000 dpm m<sup>-3</sup> (measured in three wells,  $n = 11$ ). With a radon activity of 370,000 dpm m<sup>-3</sup>, the calculated groundwater discharge would represent a fraction of 0.018 of the total water composition (river + seawater + groundwater) or about 4.6% of the river flow in January (2.2 m<sup>3</sup> s<sup>-1</sup>) and a fraction of 0.009 or about 1.1% of the river discharge in July (4.7 m<sup>3</sup> s<sup>-1</sup>). We feel that there is a high probability that any groundwater discharge consists largely of recirculated Gulf of Thailand water with some input from a shallower source than the aquifer we sampled. If the effective radon concentration were lower, the groundwater discharge values would be proportionally higher. For example, a radon activity of 100,000 dpm m<sup>-3</sup> (measured in one of the shallow wells on land close to the coast in the western portion of the upper Gulf of Thailand) would make the groundwater discharge fraction in the river equal 0.070 of the total or 20% of the river flow (10 m<sup>3</sup> s<sup>-1</sup>) in January and 0.032 or 3.7% of the river (16 m<sup>3</sup> s<sup>-1</sup>) in July. While unconfirmed, these estimates show that groundwater discharge in the river mouth may be significant. Consider, for example, that the estimated July groundwater flow (16 m<sup>3</sup> s<sup>-1</sup>) is equal to about 35% of the gauged river flow (47 m<sup>3</sup> s<sup>-1</sup>) in January.

In relative terms, the groundwater discharge represents a higher fraction of the river flow in January, although the total flux is higher in the wet season. According to salinities measured in a well sampled near the river mouth (1.2 in well W2), we believe that groundwater consists of fresh plus recirculated seawater. Seawater enters the aquifer especially at high tide and during tidal surge events as we experienced in January. Tidal inputs therefore shorten the water residence time (which could lower the resulting <sup>222</sup>Rn activity) and increase the salinity in the aquifer. Seawater dilutes the radon concentration but allows more radium to dissolve in the aquifer. Groundwater discharge in July is likely fresher because the aquifers are more saturated with freshwater from high rainfall.

The three end-member mixing calculations could also be performed using a combination of salinity and one of the tracers. However, the combination of the radon and

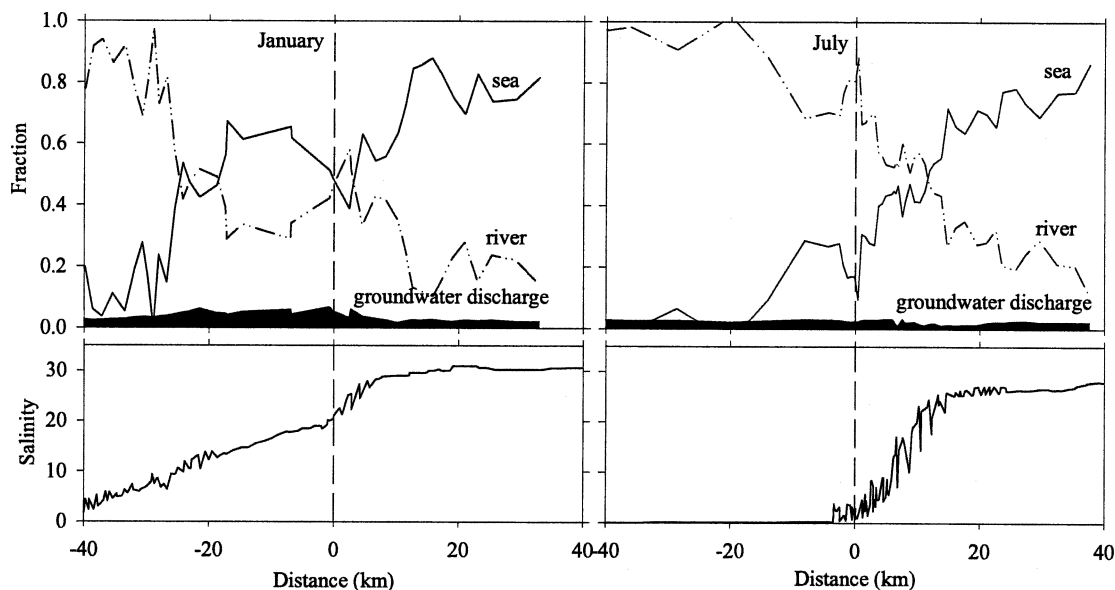


Fig. 8. Estimates of contribution of river water, seawater, and groundwater discharge to the water column plotted against distance. The fractions were calculated using a three end-member mixing model based on the respective concentrations of  $^{222}\text{Rn}$ ,  $^{224}\text{Ra}$ , and  $^{223}\text{Ra}$ . The bottom panels show the horizontal salinity profiles during the two cruises.

radium isotope AR suits the calculations better because radon can identify total groundwater inputs while the radium isotope AR helps identify different radium sources and responds more to saline flows. In addition, the groundwater discharge in this area is likely dominated by saline inflows. Figure 8 shows the composition of the water column as estimated fractions of river water, groundwater, and seawater calculated using the  $100,000 \text{ dpm m}^{-3}$  estimate as the groundwater radon concentration. The mixing curves show that there is groundwater discharge occurring in the river that appears to peak near the river mouth. The corresponding salinities measured on the transect are plotted under the mixing curves. The estimated water fractions between  $-10$  and  $-20$  km in the river in January do not agree with the measured salinities, which is probably due to the influence of the tidal surge on the isotope distribution. On the other hand, the agreement within the estuary and out onto the shelf is very good for both seasons.

*Evidence of SGD based on  $^{226}\text{Ra}$  balance*—We used the measured  $^{226}\text{Ra}$  concentrations to estimate groundwater discharge in the estuary. We constructed a  $^{226}\text{Ra}$  balance calculation based on the July data to avoid the complications caused by the tidal surge in January. We selected a pie-shaped area off the mouth of the river with an arc of  $140^\circ$  delineating the estuary from 2 to 24 km offshore, which we divided into three sections that allowed us to more precisely estimate the water depths and salinities in each section. This geometry (Fig. 1C) would most accurately portray the shape of the river plume based on examination of aerial photographs ([www.noaa.gov](http://www.noaa.gov)). The depths were estimated from a nautical map (MapSource BlueChart Pacific v5, Garmin). We calculated the volume of water by multiplying the area by the water depth in each compartment and then

summing the three portions ( $1.97 \times 10^9 \text{ m}^3$ ). Based on the  $^{226}\text{Ra}$  activity of samples collected on our transect from 2 to 24 km (average  $212 \text{ dpm m}^{-3}$ ,  $n = 11$ ), we then estimated the total  $^{226}\text{Ra}$  present in this volume ( $212 \text{ dpm m}^{-3} \times 1.97 \times 10^9 \text{ m}^3 = 4.17 \times 10^{11} \text{ dpm}$ ). We assume that this dissolved radium is derived from the river, desorption of radium from particles, groundwater discharge, and mixing with offshore seawater. Offshore water in the South China Sea at salinity 33 contains about  $80 \text{ dpm m}^{-3} \text{ }^{226}\text{Ra}$  (Nozaki et al. 2001). We used this value and the measured salinities to correct for the  $^{226}\text{Ra}$  activity in the volume that is supplied by offshore seawater ( $1.1 \times 10^{11} \text{ dpm}$ ). The difference in the total  $^{226}\text{Ra}$  and  $^{226}\text{Ra}$  activity supplied by offshore seawater is  $3.03 \times 10^{11} \text{ dpm}$ , which must be supplied by the river, desorption from particles, and groundwater discharge. From a best fit of the  $^{224}\text{Ra} : ^{223}\text{Ra}$  ages (Fig. 6) we determined that the radium age at 2 km is 3 d and at 24 km is 14 d. Therefore, the residence time of water in the volume between these two points is 11 d, and at steady state the estuarine radium flux ( $F_{\text{RaEst}}$ ) has to equal  $3.03 \times 10^{11} \text{ dpm (11 d)}^{-1}$  or  $2.8 \times 10^{10} \text{ dpm d}^{-1}$ . This flux can be expressed as

$$F_{\text{RaEst}} = Q_R C_R + Q_R C_P + Q_G C_G \quad (6)$$

where  $Q_R$  is the river discharge, which was  $430 \text{ m}^3 \text{ s}^{-1}$  in July;  $C_R$  is the dissolved  $^{226}\text{Ra}$  activity in the river ( $120 \text{ dpm m}^{-3}$ );  $C_P$  is the  $^{226}\text{Ra}$  activity that desorbs from the particles transported by the river as they encounter saline water;  $Q_G$  is the groundwater discharge; and  $C_G$  is  $^{226}\text{Ra}$  activity in the groundwater, which we estimate at  $13,500 \text{ dpm m}^{-3}$  based on the measurement in the well with salinity of 1.2.

The equation can be rearranged to solve for groundwater discharge  $Q_G$

$$Q_G = \frac{F_{\text{RaEst}} - (Q_R C_R + Q_R C_P)}{C_G} \quad (7)$$

From the particles collected on the cartridge filter at Sta. B25 we determined that the total  $^{226}\text{Ra}$  activity on the particles is  $\sim 200$  dpm  $\text{m}^{-3}$ . Since we did not measure the desorbable fraction of this radium, we will make the conservative assumption that 100% of the radium can be released to the water. This will result in a lower estimate of groundwater discharge, since this quantity is subtracted from the estuarine radium flux. Assuming that all 200 dpm  $\text{m}^{-3}$  of  $^{226}\text{Ra}$  is desorbable and released, the calculated groundwater discharge from Eq. 7 equals  $14$   $\text{m}^3$   $\text{s}^{-1}$ . A lower desorbable fraction can be estimated from the difference between the total  $^{226}\text{Ra}$  concentration on the suspended particles at zero salinity (5 dpm  $\text{g}^{-1}$ ) and  $^{226}\text{Ra}$  measured on particles that have been in contact with seawater and completely lost their desorbable radium (3.5 dpm  $\text{g}^{-1}$ ). This difference is  $\sim 1.5$  dpm  $\text{g}^{-1}$  or 60 dpm  $\text{m}^{-3}$  of released  $^{226}\text{Ra}$  ( $\sim 30\%$  of the total concentration on particles). The solution of Eq. 7 with this  $C_P$  value results in a groundwater discharge of  $19$   $\text{m}^3$   $\text{s}^{-1}$ .

While the assumption of a 100% desorbable  $^{226}\text{Ra}$  is probably not realistic, it gives a conservative lower limit of the estimate of the magnitude of the groundwater discharge. The estimated groundwater flux also depends heavily on the applied groundwater radium concentration. In this calculation we assumed that the discharging groundwater is saline and has a relatively high  $^{226}\text{Ra}$  concentration. Use of lower activities (Table 1) would make the groundwater flux even higher. Our calculated range of groundwater discharge of  $14$  to  $19$   $\text{m}^3$   $\text{s}^{-1}$  is close to our best estimate of  $16$   $\text{m}^3$   $\text{s}^{-1}$  for the July data based on the mixing model in the previous section.

Although the estimated groundwater discharge represents only a small fraction ( $\sim 4\%$ ) of the river discharge, it does represent a significant amount of groundwater seepage. With an estimated width of the river mouth of  $\sim 8$  km,  $19$   $\text{m}^3$   $\text{s}^{-1}$  translates to a unit shoreline seepage flux of over  $200$   $\text{m}^3$   $\text{m}^{-1}$   $\text{d}^{-1}$ . We measured SGD in the Gulf of Thailand using seepage meters at two sites at Sri Racha and Hua Hin as indicated in Fig. 1A (Wattayakorn et al. 2004). SGD in the Chao Phraya estuary represents a much greater flow compared with these other areas around the Gulf of Thailand ( $6$ – $22$   $\text{m}^3$   $\text{m}^{-1}$   $\text{d}^{-1}$ ), as well as other areas such as Florida ( $20$ – $30$   $\text{m}^3$   $\text{m}^{-1}$   $\text{d}^{-1}$ ; Burnett et al. 2002; Burnett and Dulaiova 2003) and Western Australia ( $3$ – $8$   $\text{m}^3$   $\text{m}^{-1}$   $\text{d}^{-1}$ ; Smith and Nield 2003), where these detailed measurements have been performed. Significant biogeochemical inputs are likely associated with these groundwater discharges. A companion study estimated nutrient discharges at the two sites where seepage meters were deployed and concluded that the groundwater seepage contributes approximately 40–50% as much dissolved inorganic nitrogen (DIN) and 60–70% of the inorganic  $\text{PO}_4$  as the surface waters of the Chao Phraya River (Wattayakorn et al. 2004).

Natural geochemical tracers proved to be very useful in assessing groundwater discharge into the Chao Phraya River and in estimating the exchange dynamics with the Gulf of Thailand. The radon and radium transects suggested that there are at least three different sources of these tracers into the river and estuary. We calculated groundwater discharge via a tracer mixing model using  $^{222}\text{Rn}$  and radium isotopes. Our estimates are  $10$  and  $16$   $\text{m}^3$   $\text{s}^{-1}$  for January and July, respectively. Another independent estimate of groundwater discharge in July using a  $^{226}\text{Ra}$  mass balance approach resulted in values between  $14$  and  $19$   $\text{m}^3$   $\text{s}^{-1}$  depending upon the estimated desorbable  $^{226}\text{Ra}$  from particles transported by the river. The groundwater inputs therefore represent about 20% of the river flow in January and 4% of the river flow in July 2004. The unit shoreline fluxes in this river-dominated area ( $\sim 200$   $\text{m}^3$   $\text{m}^{-1}$   $\text{d}^{-1}$  in July) are much higher than two other areas in the Gulf of Thailand ( $6$ – $22$   $\text{m}^3$   $\text{m}^{-1}$   $\text{d}^{-1}$ ) where these fluxes have been measured.

The Chao Phraya River is a very contaminated river with extremely high nutrient concentrations from industrial and domestic activities in Bangkok. Although nutrient concentrations measured in waters collected from seepage meters are very high (DIN  $\sim 50$ – $100$   $\mu\text{mol}$   $\text{L}^{-1}$ ;  $\text{PO}_4$   $\sim 10$   $\mu\text{mol}$   $\text{L}^{-1}$ ; Wattayakorn et al. 2004), the unit area nutrient fluxes would be smaller than the river flux since the concentrations in the river are nearly the same (mean values at flux station: DIN =  $120$  and  $60$   $\mu\text{mol}$   $\text{L}^{-1}$ ;  $\text{PO}_4$  =  $8.1$  and  $4.8$   $\mu\text{mol}$   $\text{L}^{-1}$  for January and July, respectively;  $n = 50$ ). However, seepage presumably occurs along the entire  $\sim 330$ -km shoreline, so it likely contributes a significant share of the nutrient balance to the upper Gulf of Thailand. In addition, this geochemical tracer study has shown that groundwater fluxes contribute significantly to the isotopic balance of the estuary. Presumably, other constituents in the estuarine waters are also significantly affected by groundwater inputs.

## References

- BURNETT, W. C., J. E. CABLE, AND D. R. CORBETT. 2003. Radon tracing of submarine groundwater discharge in coastal environments, p. 25–42. *In* M. Taniguchi, K. Wang and T. Gamo [eds.], Land and marine hydrogeology. Elsevier.
- , AND H. DULAIIOVA. 2003. Estimating the dynamics of groundwater input into the coastal zone via continuous radon-222 measurements. *J. Environ. Radioact.* **69**: 21–35.
- , G. KIM, AND D. LANE-SMITH. 2001a. A continuous radon monitor for assessment of radon in coastal ocean waters. *J. Radioanal. Nucl. Chem.* **249**: 167–172.
- , M. TANIGUCHI, AND J. OBERDORFER. 2001b. Measurement and significance of the direct discharge of groundwater into the coastal zone. *J. Sea Res.* **46**: 109–116.
- , AND OTHERS. 2002. Assessing methodologies for measuring groundwater discharge to the ocean. *EOS Trans. Am. Geophys. Union* **83**: 117–123.
- CABLE, J. E., G. C. BUGNA, W. C. BURNETT, AND J. P. CHANTON. 1996. Application of  $^{222}\text{Rn}$  and  $\text{CH}_4$  for assessment of groundwater discharge to the coastal ocean. *Limnol. Oceanogr.* **41**: 1347–1353.

- CHARETTE, M. A., K. O. BUESSELER, AND J. E. ANDREWS. 2001. Utility of radium isotopes for evaluating the input and transport of groundwater-derived nitrogen to a Cape Cod estuary. *Limnol. Oceanogr.* **46**: 465–470.
- DULAIIOVA, H., AND W. C. BURNETT. 2004. An efficient method for gamma spectrometric determination of  $^{226,228}\text{Ra}$  via Mn fibers. *Limnol. Oceanogr. Methods* **2**: 256–261.
- , R. PETERSON, W. C. BURNETT, AND D. LANE-SMITH. 2005. A multidetector continuous monitor for assessment of  $^{222}\text{Rn}$  in the coastal ocean. *J. Radioanal. Nucl. Chem.* **263**: 361–365.
- KELLY, R. P., AND S. B. MORAN. 2002. Seasonal changes in groundwater input to a well-mixed estuary estimated using radium isotopes and implications for coastal nutrient budgets. *Limnol. Oceanogr.* **47**: 1796–1807.
- KJERFVE, B. 1979. Measurement and analysis of water current, temperature, salinity and density, p. 186–216. *In* K. R. Dyer [ed.], *Hydrography and sedimentation in estuaries*. Cambridge Univ. Press.
- KREST, J. M., W. S. MOORE, AND RAMA. 1999.  $^{226}\text{Ra}$  and  $^{228}\text{Ra}$  in the mixing zones of the Mississippi and Atchafalaya Rivers: Indicators of groundwater input. *Mar. Chem.* **64**: 129–152.
- LI, Y.-H., G. MATHIEU, P. BISCAYE, AND H. J. SIMPSON. 1977. The flux of  $^{226}\text{Ra}$  from estuarine and continental shelf sediments. *Earth Planet. Sci. Lett.* **37**: 237–241.
- MACINTYRE, S., R. WANNINKHOF, AND J. P. CHANTON. 1995. Trace gas exchange across the air-sea interface in freshwater and coastal marine environments, p. 52–97. *In* P. A. Matson and R. C. Harris [eds.], *Biogenic trace gases: Measuring emissions from soil and water*. Blackwell Science Ltd.
- MOORE, W. S. 1976. Sampling  $^{228}\text{Ra}$  in the deep ocean. *Deep-Sea Res. Oceanogr. Abstr.* **23**: 647–651.
- . 1996. Large groundwater inputs to coastal waters revealed by  $^{226}\text{Ra}$  enrichments. *Nature* **380**: 612–614.
- . 1997. High fluxes of radium and barium from the mouth of the Ganges-Brahmaputra River during low river discharge suggest large groundwater source. *Earth Planet. Sci. Lett.* **150**: 141–150.
- . 2000. Ages of continental shelf waters determined from  $^{223}\text{Ra}$  and  $^{224}\text{Ra}$ . *J. Geophys. Res.* **105**: 22,117–22,122.
- , AND R. ARNOLD. 1996. Measurement of  $^{223}\text{Ra}$  and  $^{224}\text{Ra}$  in coastal waters using delayed coincidence counter. *J. Geophys. Res.* **101**: 1321–1329.
- , H. ASTWOOD, AND C. LINDSTROM. 1995. Radium isotopes in coastal waters on the Amazon shelf. *Geochim. Cosmochim. Acta* **59**: 4285–4298.
- , AND J. KREST. 2004. Distribution of  $^{223}\text{Ra}$  and  $^{224}\text{Ra}$  in the plumes of the Mississippi and Atchafalaya Rivers and the Gulf of Mexico. *Mar. Chem.* **86**: 105–119.
- NOZAKI, Y., Y. YAMAMOTO, T. MANAKA, H. AMAKAWA, AND A. SNIDVONGS. 2001. Dissolved barium and radium isotopes in the Chao Phraya River estuarine mixing zone in Thailand. *Cont. Shelf Res.* **21**: 1435–1448.
- SMITH, A. J., AND S. P. NIELD. 2003. Groundwater discharge from the superficial aquifer into Cockburn Sound Western Australia: Estimation by inshore water balance. *Biogeochemistry* **66**: 125–144.
- STANSFIELD, K., AND C. GARRETT. 1977. Implications of the salt and heat budgets of the Gulf of Thailand. *J. Mar. Res.* **55**: 935–963.
- SUN, Y., AND T. TORGERSEN. 2001. Adsorption-desorption reactions and bioturbation transport of  $^{224}\text{Ra}$  in marine sediments: A one-dimensional model with applications. *Mar. Chem.* **74**: 227–243.
- TANIGUCHI, M., W. C. BURNETT, J. E. CABLE, AND J. V. TURNER. 2002. Investigation of submarine groundwater discharge. *Hydrol. Proc.* **16**: 2115–2129.
- WATTAYAKORN, G., W. C. BURNETT, M. TANIGUCHI, P. SOJISUPORN, AND S. RUNGSUPA. 2004. Contribution of carbon and nutrient species into SE Asian waters via submarine groundwater discharge [Internet]. The Southeast Asia Regional Committee for START (SARCS), Carbon pilot research project, Final report; 2004 Oct [accessed 2006 April 15] 35 p. Available from <http://www.sarcs.org/new/initiated/Carbon/Carbon%20Pilot%20Project%20Final%20Report/Thailand%20Final%20Report.pdf>

Received: 1 August 2005

Accepted: 20 March 2006

Amended: 29 March 2006